Regular Article

Anna Borowska*

Stadiums based on curvilinear geometry: Approximation of the ellipsoid offset surface

https://doi.org/10.1515/eng-2022-0392
received October 03, 2022; accepted November 30, 2022

Abstract: This article provides an effective method of determining the coordinates of points and the angles for various surfaces approximating the ellipsoid surface. The stands of the stadium (with a capacity of up to 82,000 seats) with rows shaped by ellipse arcs were designed (in accordance with the European Standard EN 13200-1). An algorithm was proposed to determine the optimal height of the ring steps (with the guarantee of unobstructed vision of the entire playing field from each seat of the stands). The second algorithm ensures a comfortable space in each individual seating place in the stands (deviation of the depth of the row generated by ellipse arcs did not exceed 0.000009 m at any place of the stands). This article encourages readers to program DXF files (read in the AutoCAD system) to streamline design work.

Keywords: offset surface, ellipsoid, stadium stands, DXF file

1 Introduction

Architectural objects are based on sophisticated curvilinear geometry, and although they are not the cheapest, they increasingly appear on city maps (Sydney Opera House, Sky Towers (Abu Dhabi), Beijing National Grand Theatre, Jumeirah Beach Hotel (Dubai)). Such investments will attract tourists over the following years. So, good ideas for reducing the costs of their construction are very important.

To design a structure based on an ellipsoid $S(u, v)$, the coordinates of points of other surfaces approximating the surface $S(u, v)$ are necessary (Figures 1 and 2). The approximating surface can be an offset surface or another ellipsoid (with the desired properties) concentric with the base surface. Sections 2.1–2.4 provide mathematical formulas and the effective methodology for acquiring angles and coordinates of points of different surfaces approximating the ellipsoid surface.

The aim of this study is to program (according to the European Standard EN 13200-1) stadium stands with rows shaped by ellipse arcs. Modern stadium stands are designed in such a way as to place tens of thousands of people in one space and provide them with an uninterrupted view of the entire playing field and a comfortable space in an individual seating place. The problem of providing tens of thousands of people with an unobstructed view of the entire playing field was solved using the line of sight correction (LSC) algorithm (compared with Section 3.3) and the ball vision verification (BVV) algorithm (compared with Section 3.4). The problem of providing them with a comfortable space in an individual seating place was resolved using the row depth correction (RDC) algorithm (compared with Section 3.6). To design and verify the presented algorithms, tests were carried out for different variants of stands.

All figures were programed in C++ (in Visual Studio 2019), saved in DXF format (compared with ref. [1]), and exported (in the AutoCAD system) to DWG file (a standard file format for CAD).

2 The approximation of the ellipsoid offset surface

2.1 Mathematical formulas

Lemma 1. (compared with [2,3], p. 44) *If* $\arccos(x) = \arcsin(y)$ *and* $x + y > 0$, *then* $x^2 + y^2 = 1$.

Let $S(u,v) = (x(u,v), y(u,v), z(u,v))$ $(u \in [u_1, u_2], v \in [v_1, v_2])$ be a parametric representation of a smooth surface in three-dimensional space. The unit normal vector to the

* **Corresponding author: Anna Borowska,** Department of Theoretical Computer Science, Faculty of Computer Science, Bialystok University of Technology, ul.Wiejska 45a, 15-351, Bialystok, Poland, e-mail: a.borowska@pb.edu.pl

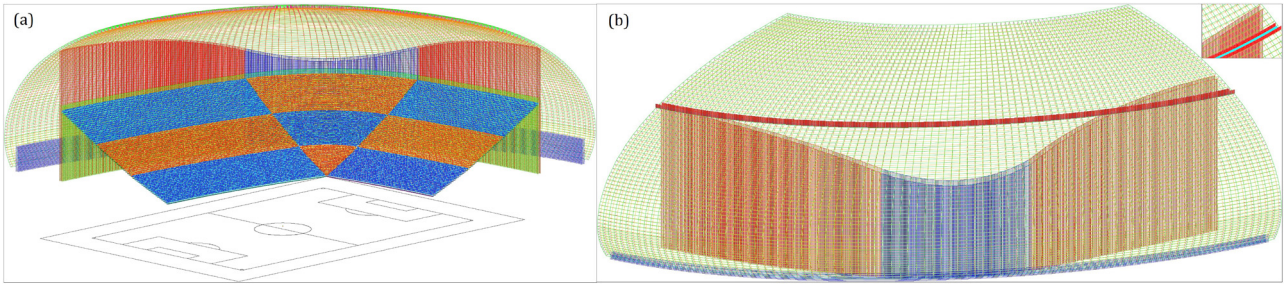

Figure 1: (a) Three-tier stadium with covered stands and (b) the ellipsoid-shaped elevation of the stadium with a footbridge.

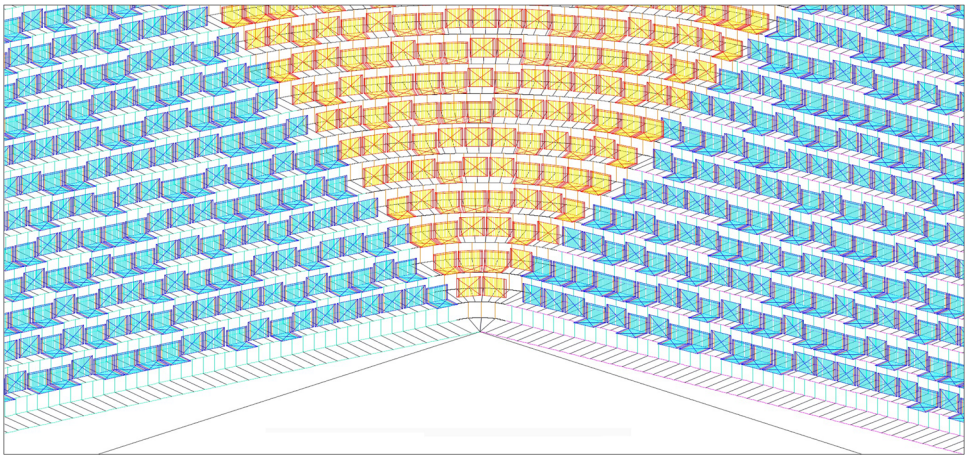

Figure 2: The stands in the corner (a close-up).

surface S at the point R_0 is of the following form (compared with ref. [4], p. 28)

$$\vec{n}_{\text{unv}}(u_0, v_0) = \frac{\vec{r_u}(u_0, v_0) \times \vec{r_v}(u_0, v_0)}{|\vec{r_u}(u_0, v_0) \times \vec{r_v}(u_0, v_0)|}, \text{ where}$$

$$\vec{r_u}(u_0, v_0) = \left[\frac{\partial x}{\partial u}, \frac{\partial y}{\partial u}, \frac{\partial z}{\partial u}\right]_{u=u_0, v=v_0}, \text{ and}$$

$$\vec{r_v}(u_0, v_0) = \left[\frac{\partial x}{\partial v}, \frac{\partial y}{\partial v}, \frac{\partial z}{\partial v}\right]_{u=u_0, v=v_0}$$

are the tangent vectors to the surface S at the point R_0.

For a given smooth surface S, we can define an offset $\text{off}_d S$ at distance d (compared with ref. [5], p. 341) as follows. On each surface normal, we mark the two points that are at a constant distance d from the surface S. The set of all of these points forms the offset surface $\text{off}_d S$. The offset surface $\text{off}_d S(u, v)$ at distance d to $S(u, v)$ is obtained as follows:

$$\text{off}_d S(u, v) = S(u, v) \pm d \cdot \vec{n}_{\text{unv}}(u, v).$$

Practical applications of the offset surfaces (offset curves) are described in refs [4,6,7].

Let S, S_1, and S_2 be the concentric ellipsoid surfaces defined as follows (compared with ref. [8], p. 238).

$$S(u, v): \quad x = a\cos(u)\sin(v), \quad y = b\sin(u)\sin(v), \quad z = c\cos(v), \; u \in [0, 2\pi], \; v \in [0, \pi], \tag{1}$$

$$S_1(u, v): \quad x = (a + d)\cos(u)\sin(v), \quad y = (b + d)\sin(u)\sin(v), \quad z = (c + d)\cos(v), \tag{2}$$

$$S_2(u, v): \quad x = (a - d)\cos(u)\sin(v), \quad y = (b - d)\sin(u)\sin(v), \quad z = (c - d)\cos(v). \tag{3}$$

Let us assume that P is any point on the ellipsoid S (Figure 3) and l is the normal line to S at the point P. Points P_1 and P_2 lie on the normal line l at distance d from P. Q_1, Q_2 are the intersection points of the normal l with ellipsoids S_1 and S_2, respectively. Ellipsoids S_1 and S_2 do not keep a constant distance d relative to the ellipsoid S (distances $d_{P_1Q_1} = |\overline{P_1Q_1}| > 0$ and $d_{P_2Q_2} = |\overline{P_2Q_2}| > 0$) at points not lying on the axes of the coordinate system (Figure 3).

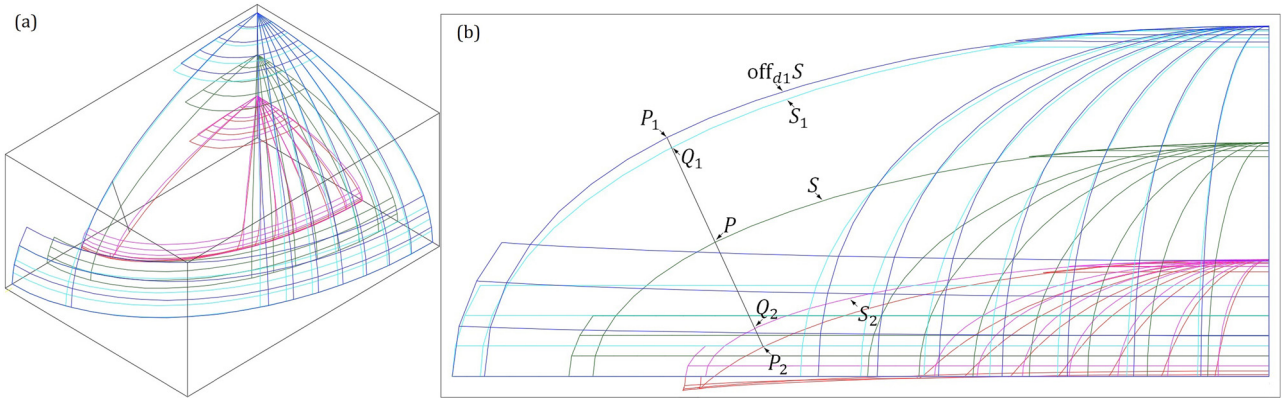

Figure 3: The arrangement of points and surfaces S, S_1, S_2, off$_{d1}S$, off$_{d2}S$.

2.2 The coordinates of points P_1 and P_2

Let us take the parametric equations (1) of the ellipsoid $S(u, v)$. The coordinates of points P_1 and P_2 lying on the normal l to the ellipsoid $S(u, v)$ (at the point $P(x_P, y_P, z_P)$) and distant from P by the length d can be determined using the following equation of the offset surface off$_d S(u, v)$.

$$\text{off}_d S(u,v): \ [X,Y,Z] = [x,y,z] \pm \frac{d[-bc\cos(u)\sin(v), -ac\sin(u)\sin(v), -ab\cos(v)]}{\sqrt{(bc\cos(u)\sin(v))^2 + (ac\sin(u)\sin(v))^2 + (ab\cos(v))^2}}. \tag{4}$$

The coordinates of points P_1 and P_2 are as follows:

$$x_{P_1} = x_P + \frac{dbcx_P}{aw}, \ y_{P_1} = y_P + \frac{dacy_P}{bw}, \ z_{P_1} = z_P + \frac{dabz_P}{cw}, \tag{5}$$

$$x_{P_2} = x_P - \frac{dbcx_P}{aw}, \ y_{P_2} = y_P - \frac{dacy_P}{bw}, \ z_{P_2} = z_P - \frac{dabz_P}{cw}, \tag{6}$$

where

$$w = \sqrt{(bc\cos(u_0)\sin(v_0))^2 + (ac\sin(u_0)\sin(v_0))^2 + (ab\cos(v_0))^2} \tag{7}$$

$$x_P = a\cos(u_0)\sin(v_0), \ y_P = b\sin(u_0)\sin(v_0), \ z_P = c\cos(v_0). \tag{8}$$

In practical applications, the (smaller) offset surface off$_{d2}S(u, v)$ requires correction (Figure 4(a)), because a part of this surface (for $u, v \in [0, \pi/2]$) is below the OXY plane. To get the coordinates $x_{P_2} \geq 0$, $y_{P_2} \geq 0$, $z_{P_2} \geq 0$ (for $u, v \in [0, \pi/2]$), we have to take into account the following conditions $x_{P_2} \geq 0$ iff $w \geq \frac{dbc}{a}$, $y_{P_2} \geq 0$ iff $w \geq \frac{dac}{b}$, $z_{P_2} \geq 0$ iff $w \geq \frac{dab}{c}$ (Figure 4(b and c)). The green line segments (perpendicular to the red surface $S(u, v)$), one end of which is (in Figure 4(a)) below the OXY plane, were trimmed (in Figure 4(b and c)) at points with the coordinates x_{P_2}, y_{P_2}, z_{P_2} (for $w = \frac{dab}{c}$). The fragment of the (blue) surface (mesh) off$_{d2}S(u, v)$ was reduced to the part above the OXY plane (Figure 4(b and c)) using the approximation algorithm (using a "divide and conquer" strategy).

2.3 The coordinates of points Q_1 and T_1

Let $S(u, v)$ and $S_1(\varphi, \xi)$ $(u, \varphi \in [0, 2\pi], \ v, \xi \in [0, \pi])$ be the concentric ellipsoids defined in (1) and (2). Let us assume that $u_0, v_0, \varphi, \xi \in [0, \pi/2]$ and set the parameter h, which gives the coordinates of the point Q_1 (an intersection of the normal line l to the surface $S(u, v)$ at the point P with the surface $S_1(\varphi, \xi)$):

$$\begin{cases} \cos(u_0)\sin(v_0)\left(a + \frac{hdbc}{w}\right) = (a+d)\cos(\varphi)\sin(\xi) \\ \sin(u_0)\sin(v_0)\left(b + \frac{hdac}{w}\right) = (b+d)\sin(\varphi)\sin(\xi) \\ \cos(v_0)\left(c + \frac{hdab}{w}\right) = (c+d)\cos(\xi). \end{cases}$$

Hence and from Lemma 1, we have $Ah^2 + Bh + C = 0$, where

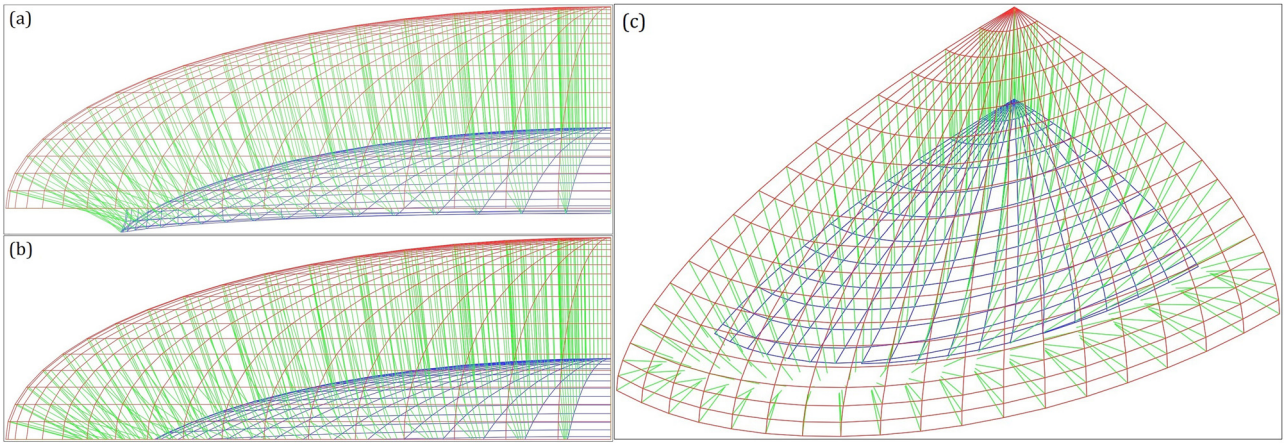

Figure 4: A fragment of the ellipsoid $S(u, v)$ and the offset surface $\mathrm{off}_{d2}S(u, v)$ ($a = 60$, $b = 40$, $c = 20$, $d = 12$): (a) a part of the surface $\mathrm{off}_{d2}S(u, v)$ is below the *OXY* plane and (b and c) a fragment of the surface $\mathrm{off}_{d2}S(u, v)$ is above the *OXY* plane (after removal of the part of the surface $\mathrm{off}_{d2}S(u, v)$ that was below the *OXY* plane).

$$A = \frac{d^2(A_1b^2c^2 + B_1a^2c^2 + C_1a^2b^2)}{w^2},$$
$$B = \frac{2abcd(A_1 + B_1 + C_1)}{w},$$
$$C = A_1a^2 + B_1b^2 + C_1c^2 - 1 \text{ for}$$
$$A_1 = \left(\frac{\cos(u_0)\sin(v_0)}{(a + d)}\right)^2, \quad B_1 = \left(\frac{\sin(u_0)\sin(v_0)}{(b + d)}\right)^2,$$
$$C_1 = \left(\frac{\cos(v_0)}{(c + d)}\right)^2 \text{ and } w \text{ (compared with (7)).}$$

Therefore (for $\Delta = B^2 - 4AC > 0$), we have $h_1 = \frac{-B + \sqrt{\Delta}}{2A}$ (the parameter for the point Q_1) and $h_2 = \frac{-B - \sqrt{\Delta}}{2A}$. Finally,

$$x_{Q_1} = \cos(u_0)\sin(v_0)\left(a + \frac{h_1dbc}{w}\right),$$
$$y_{Q_1} = \sin(u_0)\sin(v_0)\left(b + \frac{h_1dac}{w}\right),$$
$$z_{Q_1} = \cos(v_0)\left(c + \frac{h_1dab}{w}\right).$$

Let l be the normal line to the surface $S(u, v)$ at the point $P(x_P, y_P, z_P)$ (compared with (8)). The line l passes through the point $P_1(x_{P_1}, y_{P_1}, z_{p_1})$ (compared with (5)). The line t is the orthographic projection of the line l onto the plane (containing the point P and parallel to the *OXY* plane). Let us assume that $u_0, v_0, \varphi, \xi \in [0, \pi/2]$ and set the parameter h, which gives the coordinates of the point $T_1(x_{T_1}, y_{T_1}, z_{T_1})$ (an intersection of the line t with the surface $S_1(\varphi, \xi)$ (compared with (2))):

$$\begin{cases} x_P + h\left(x_{P_1} - x_P\right) = (a + d)\cos(\varphi)\sin(\xi) \\ y_P + h(y_{P_1} - y_P) = (b + d)\sin(\varphi)\sin(\xi) \\ z_P = (c + d)\cos(\xi). \end{cases}$$

Hence and from Lemma 1, we obtain $Ah^2 + Bh + C = 0$, where $A = A_1(x_{P_1} - x_P)^2 + B_1(y_{P_1} - y_P)^2$, $B = 2(A_1x_P(x_{P_1} - x_P) + B_1y_P(y_{P_1} - y_P))$, and $C = A_1x_P^2 + B_1y_P^2 - 1$ for $A_1 = \frac{1}{(a+d)^2\sin^2(\xi)}$, $B_1 = \frac{1}{(b+d)^2\sin^2(\xi)}$, and $\xi = \arccos\left(\frac{z_P}{c+d}\right)$. Therefore (for $\Delta = B^2 - 4AC > 0$), we have $h_1 = \frac{-B + \sqrt{\Delta}}{2A}$ (the parameter for the point T_1) and $h_2 = \frac{-B - \sqrt{\Delta}}{2A}$. Finally, for w (compared with (7)):

$$x_{T_1} = \cos(u_0)\sin(v_0)\left(a + \frac{h_1dbc}{w}\right),$$
$$y_{T_1} = \sin(u_0)\sin(v_0)\left(b + \frac{h_1dac}{w}\right),$$
$$z_{T_1} = z_P = c\cos(v_0).$$

Figure 5(a) shows a fragment of the (red) ellipsoid $S(u, v)$, the (blue) ellipsoid $S_1(u, v)$ and the (green) offset surface $\mathrm{off}_{d1}S(u, v)$, yellow line segments $\overline{PP_1}$ and (pink) line segments $\overline{PQ_1}$. Figure 5(b) presents a fragment of the (orange) ellipsoid $S(u, v)$, the (green) ellipsoid $S_1(u, v)$, (blue) horizontal line segments $\overline{PT_1}$, and (pink) line segments $\overline{PQ_1}$. The orthographic projections of the segments $\overline{PQ_1}$ and $\overline{PT_1}$ onto the *OXY* plane lie on one line.

2.4 The coordinates of points Q_2 and T_2

Let $S(u, v)$ and $S_2(\varphi, \xi)$ ($u, \varphi \in [0, 2\pi]$, $v, \xi \in [0, \pi]$, $a, b, c > d$) be the concentric ellipsoids defined in (1) and (3). Let us assume that $u_0, v_0, \varphi, \xi \in [0, \pi/2]$ and set the parameter h giving the coordinates of the point Q_2 (an intersection of the normal line l to the surface $S(u, v)$ at the point P with the surface $S_2(\varphi, \xi)$):

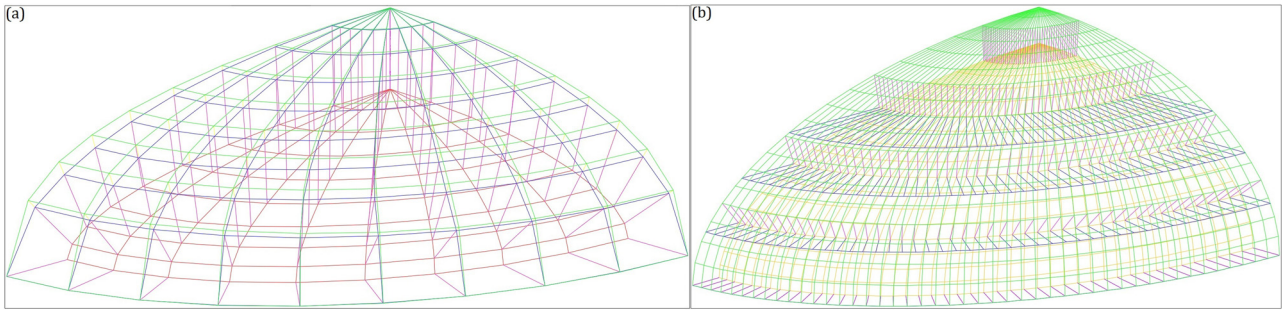

Figure 5: Fragments of the surfaces $S(u, v)$, $S_1(u, v)$, and $\mathrm{off}_{d1}S(u, v)$ (a) for $a = 80$, $b = 60$, $c = 15$, $d = 15$ and (b) for $a = 60$, $b = 40$, $c = 20$, $d = 5$.

$$\begin{cases} \cos(u_0)\sin(v_0)\left(a - \dfrac{hdbc}{w}\right) = (a - d)\cos(\varphi)\sin(\xi) \\ \sin(u_0)\sin(v_0)\left(b - \dfrac{hdac}{w}\right) = (b - d)\sin(\varphi)\sin(\xi) \\ \cos(v_0)\left(c - \dfrac{hdab}{w}\right) = (c - d)\cos(\xi). \end{cases}$$

Hence and from Lemma 1, we obtain the equation $Ah^2 + Bh + C = 0$, where

$$A = \frac{d^2(A_1b^2c^2 + B_1a^2c^2 + C_1a^2b^2)}{w^2},$$
$$B = \frac{-2dabc(A_1 + B_1 + C_1)}{w},$$
$$C = A_1a^2 + B_1b^2 + C_1c^2 - 1 \text{ for } A_1 = \left(\frac{\cos(u_0)\sin(v_0)}{(a - d)}\right)^2,$$
$$B_1 = \left(\frac{\sin(u_0)\sin(v_0)}{(b - d)}\right)^2,$$
$$C_1 = \left(\frac{\cos(v_0)}{(c - d)}\right)^2 \text{ and } w \text{ (compared with (7)).}$$

Therefore (for $\Delta = B^2 - 4AC > 0$), we have $h_1 = \frac{-B + \sqrt{\Delta}}{2A}$, and $h_2 = \frac{-B - \sqrt{\Delta}}{2A}$ (the parameter for the point Q_2). Finally:

$$\begin{aligned} x_{Q_2} &= \cos(u_0)\sin(v_0)\left(a - \frac{h_2dbc}{w}\right), \\ y_{Q_2} &= \sin(u_0)\sin(v_0)\left(b - \frac{h_2dac}{w}\right), \\ z_{Q_2} &= \cos(v_0)\left(c - \frac{h_2dab}{w}\right). \end{aligned} \tag{9}$$

Remark 1. By using the equalities (9) to determine the coordinates x_{Q_2}, y_{Q_2}, z_{Q_2} (for $u, v \in [0, \pi/2]$), we obtain $x_{Q_2} \geq 0$ iff $h_2 \leq \frac{aw}{dbc}$ and $y_{Q_2} \geq 0$ iff $h_2 \leq \frac{bw}{dac}$ and $z_{Q_2} \geq 0$ iff $h_2 \leq \frac{cw}{dab}$.

Let l be the normal line to the surface $S(u, v)$ at the point $P(x_P, y_P, z_P)$ (compared with (8)). The line l passes through the point $P_2(x_{P_2}, y_{P_2}, z_{p_2})$ (compared with (6)). The line t is the orthographic projection of the line l onto the plane (containing the point P and parallel to the OXY plane). Let us assume that $u_0, v_0, \varphi, \xi \in [0, \pi/2]$. The coordinates of the point $T_2(x_{T_2}, y_{T_2}, z_{T_2})$ (an intersection of the line t with the surface $S_2(\varphi, \xi)$ (compared with (3))) are as follows:

$$\begin{aligned} x_{T_2} &= \cos(u_0)\sin(v_0)\left(a - \frac{h_2dbc}{w}\right), \\ y_{T_2} &= \sin(u_0)\sin(v_0)\left(b - \frac{h_2dac}{w}\right), \\ z_{T_2} &= z_P = c\cos(v_0), \end{aligned}$$

where $h_2 = \frac{-B - \sqrt{\Delta}}{2A}$ (for $\Delta = B^2 - 4AC > 0$),

$$A = A_1\left(x_{P_2} - x_P\right)^2 + B_1(y_{P_2} - y_P)^2,$$
$$B = 2\left(A_1x_P\left(x_{P_2} - x_P\right) + B_1y_P(y_{P_2} - y_P)\right),$$
$$C = A_1x_P^2 + B_1y_P^2 - 1, \quad A_1 = \frac{1}{(a - d)^2\sin^2(\xi)},$$
$$B_1 = \frac{1}{(b - d)^2\sin^2(\xi)}, \quad \xi = \arccos\left(\frac{z_P}{c - d}\right),$$
$$w \text{ (compared with (7)).}$$

Figure 6(a) shows a fragment of the (red) ellipsoid $S(u, v)$, the (green) ellipsoid $S_2(u, v)$, the (blue) offset surface $\mathrm{off}_{d2}S(u, v)$, (black) line segments $\overline{PP_2}$, and (pink) line segments $\overline{PQ_2}$. Figure 6(b) presents a fragment of the (green) ellipsoid $S(u, v)$, the (orange) ellipsoid $S_2(u, v)$, (blue) horizontal line segments $\overline{PT_2}$, and (pink) line segments $\overline{PQ_2}$.

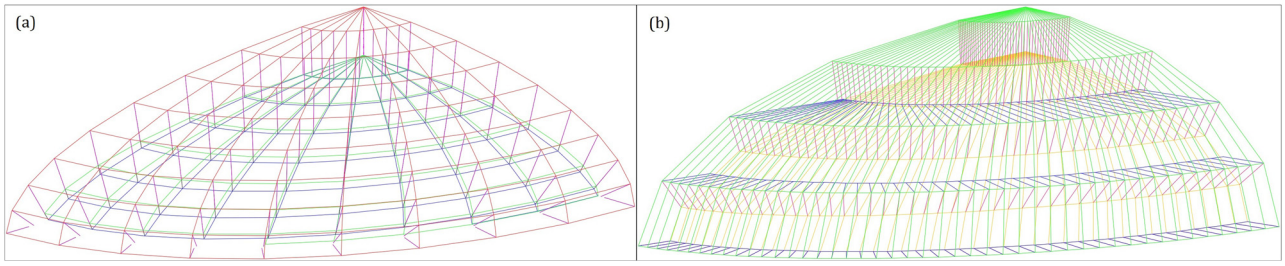

Figure 6: Fragments of the surfaces $S(u, v)$, $S_2(u, v)$, and $\mathrm{off}_{d2}S(u, v)$: (a) for $a = 80$, $b = 60$, $c = 20$, $d = 8$, (b) for $a = 60$, $b = 40$, $c = 20$, $d = 5$.

3 Stadiums based on curvilinear geometry

The form of the stands of a contemporary stadium is shaped in such a way as to place tens of thousands of people in one space and provide them with: an uninterrupted view of the entire playing field, a comfortable space in an individual seating place, and safe conditions for communication and evacuation (compared with ref. [9], p. 97). The paper proposes the construction of the stadium stands (in accordance with the guidelines and standards [10,11]) based on curvilinear geometry (i.e., with rows along the ellipse arcs) and with a constant height of the ring steps (different for each ring).

3.1 Symbols and dimensions of the stadium

The following dimensions of the stadium comply with the standards [10,11].

$2dx = 105$ m ($2dy = 68$ m) – the length (and width) of the playing field; $ax = 10$ m ($ay = 8.5$ m) – the nominal width of the auxiliary area on the ends (on the sides); $2dax \times 2day = 130$ m $\times$ 90 m – the arena dimensions ($dax = dx + ax + 2.5$ m, $day = dy + ay + 2.5$ m "The normative dimensions of the arena of a modern football stadium cannot be smaller than 130 m $\times$ 90 m" (compared with ref. [9], p. 11)), $S = 0.8$ m – the depth of a row; $G = 0.25$ m – the distance of the eye point from the back edge of a row; $\Delta Ok = S - G = 0.55$ m, $HOs = 1.2$ m – the (normative) eye-height for a sitting position (compared with ref. [9], p. 97); $Cx = 0.12$ m – the distance from the eye point to the top of the head (compared with ref. [9], p. 133); $\Delta y \in \{0.5, 1.0, \ldots, 20\}$ ($\Delta x \in \{0.5, 1.0, \ldots, 20\}$) – increment of the semi-minor (semi-major) axis of an ellipse e_{B_i} (e_{A_i}) for the side stands (for the stands behind the goal).

The stadium stands consist of three rings (I, II, and III) and are divided into parts as follows: the side stands (BA and BB), the stands behind the goal (AA and AB), and the stand in the corner (C) (Figure 7(a and b)). Three types of arcs were used for the design: the arcs of concentric ellipses e_{B_i} (for stands BA and BB), the arcs of concentric ellipses e_{A_i} (for stands AA and AB), and the arcs of concentric circles e_{C_i} (for the stand C). The center of the ellipses is in the center of the pitch, and the center of the circles is in the corners of the auxiliary arena.

In the side stands: the arc of the ellipse e_{B_0} shapes the front edge of the first row, the arcs of ellipses e_{B_i} (for $i \in [1, R]$, where $n + m + k = R$ – the number of rows in the stands) define the back edges of the consecutive rows, and the arcs of ellipses $e_{\Delta B_i}$ (for $i \in [1, R]$) model the eye lines in the consecutive rows.

e_{B_0}: $x_{B_0} = a_{B_0}\cos(u)$, $y_{B_0} = b_{B_0}\sin(u)$, where $b_{B_0} = day + \Delta y$ and $a_{B_0} = \frac{dax}{\cos(t_1)}$ for $t_1 = \arcsin\left(\frac{day}{b_{B_0}}\right)$, $u \in [t_1, 90^\circ]$ (the ellipse e_{B_0} reaches the point (dax, day) for the angle t_1),

$$e_{B_i}: \; x_{B_i} = a_{B_i}\cos(u), \; y_{B_i} = b_{B_i}\sin(u), \text{ where}$$
$$a_{B_i} = a_{B_0} + iS, \; b_{B_i} = b_{B_0} + iS, \; u \in [t_1, 90^\circ],$$
$$e_{\Delta B_i}: \; x_{\Delta B_i} = a_{\Delta B_i}\cos(u), \; y_{\Delta B_i} = b_{\Delta B_i}\sin(u), \text{ where}$$
$$b_{\Delta B_i} = day + \Delta y + \Delta Ok + (i-1)S,$$
$$a_{\Delta B_i} = \frac{dax}{\cos(t_1)} + \Delta Ok + (i-1)S \text{ for } u \in [t_1, 90^\circ].$$

The arcs of ellipses e_{A_i} ($i \in [0, R]$), $e_{\Delta A_i}$ ($i \in [1, R]$) (for $u \in [0^\circ, v_1]$, $v_1 = \arccos\left(\frac{dax}{a_{A_0}}\right)$, and $a_{A_0} = dax + \Delta x$, (the ellipse e_{A_0} reaches the point (dax, day) for the angle v_1)) shaping the stands behind the goal were defined in a similar way.

The arcs of circles e_{C_i} ($i \in [1, R]$) model the back edges of the rows of the stand in the corner:

$$e_{C_i}: \; x_{C_i} = a_{C_i}\cos(u) + dax, \; y_{C_i} = a_{C_i}\sin(u) + day, \text{ where}$$
$$a_{C_i} = iS, \; u \in [v_1, t_1].$$

The arcs of circles $e_{\Delta C_i}$ ($i \in [1, R]$) model the eye lines in the rows of the stand in the corner:

$$e_{\Delta C_i}: \; x_{\Delta C_i} = a_{\Delta C_i}\cos(u) + dax, \; y_{\Delta C_i} = a_{\Delta C_i}\sin(u) + day,$$
$$\text{where } a_{\Delta C_i} = \Delta Ok + (i-1)S, \; u \in [v_1, t_1].$$

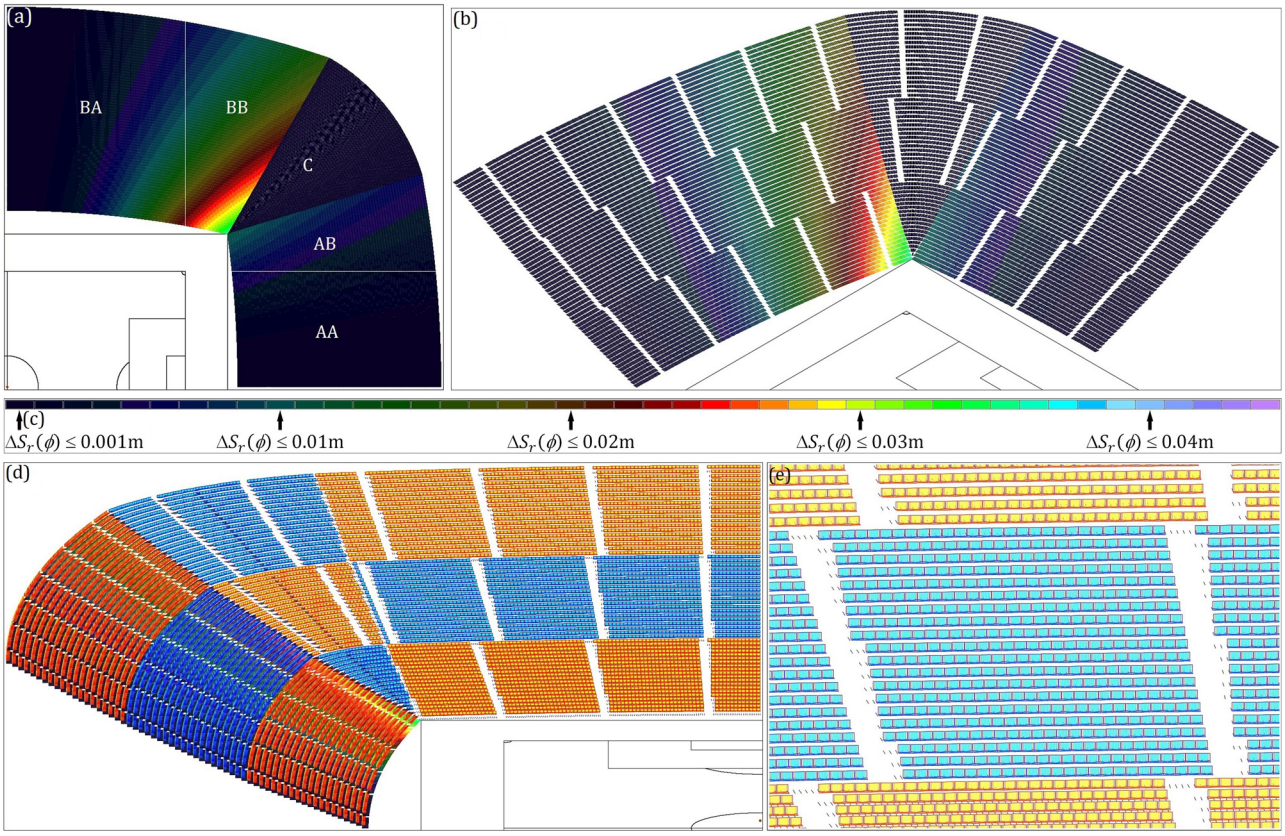

Figure 7: The stadium stands (for $\Delta x = 3$ m, $\Delta y = 7$ m, $n, m, k = 20$): (a) depth of the rows (top view), (b) depth of the rows (SW Isometric view), (c) color palette, (d) the arrangement of seats in the stands, and (e) a view of a sector in the stand behind the goal.

3.2 Depth of a row

Remark 2. While determining the length of the ellipse arc, we obtain an elliptic integral that cannot be expressed by elementary functions (compared with ref. [12], p. 315–318). When designing the stadium stands, the length of the ellipse arc, measured along a broken line (composed of equal segments) inscribed in the ellipse arc, is more useful.

Symbols: $S_r(\phi)$ – the depth of a row r (for the angle ϕ) measured along the perpendicular segment to the back edge of the row; $\Delta S_r(\phi) = S - S_r(\phi)$ – row depth deficit (for the angle ϕ).

The values of $S_r(\phi)$ were determined for the side stands and the stands behind the goal (for three rings). It was assumed that each ring consists of 25 rows. To plot the back edges of the rows, the arcs of ellipses e_{B_i} (for the side stands) and e_{A_i} (for the stands behind the goal) (for $i \in [1, R]$ (compared with Section 3.1) and $\Delta x, \Delta y \in \{0.5, 1, 1.5, 2, \ldots, 20\}$) were used. The values of $S_r(\phi)$ were calculated as the lengths of the line segments $|\overline{P_iQ_2}|$ for $i \in [1, R]$ (the point P_i lies on the ellipse e_{B_i} (e_{A_i}) for the angle ϕ). Points P_i were measured every $\Delta\phi_i$ (corresponding to a length of 0.25 m) along a broken line inscribed in the arc of the ellipse e_{B_i} (e_{A_i}) defining the back edge of the row. That is, on the ellipse arc, segments with a length 0.25 m were measured (using an approximation method), and the angles $\Delta\phi_i$ were calculated. Coordinates of the point Q_2 (for the determined P_i) were calculated from the formula (9) for $d = 0.8$ m, $c = 1$, and $v_0 = 90^\circ$. The results are presented in Tables 1 and 2 and in Figures 7 and 8.

Figure 7 shows the stadium stands plotted for unfavorable values $\Delta x = 3$ m and $\Delta y = 7$ m (for $\Delta x = 3$ m, we obtain $S_1(v_1) = 0.789478$ m and $\Delta S_1 > 0.01$ m for 1.25 m (for 2.5 seats), and for $\Delta y = 7$ m, we have $S_1(t_1) = 0.765147$ m and $\Delta S_1 > 0.03$ m for 5 m (for 10 seats) (compared with Tables 1 and 2)). The floor in the consecutive rows was painted along the line segments perpendicular to the back edge of the row in a color determined by the length of the line segment (according to the color palette) (see Figure 7(c)). Figure 7(a and b) shows that the greatest deficit $\Delta S_1(\phi) = 0.034853$ m occurred in the

Table 1: Test results for the side stands (for $\Delta y \in \{0.5, 1, 1.5, 2, 3, 5, 7, 10, 15, 20\}$, $n, m, k = 25$)

Δy (m)	**0.5**	**1**	**1.5**	**2**	**3**	**5**	**7**	**10**	**15**	**20**
b_{B_1} (m)	46.3	46.8	47.3	47.8	48.8	50.8	52.8	55.8	60.8	65.8
a_{B_1} (m)	440.45849	314.23717	258.79431	226.01759	187.58951	149.92023	130.51249	113.85143	99.07076	90.87730
$t_1[\circ]$	81°29′53″	78°1′52″	75°24′27″	73°13′31″	69°38′9″	64°9′29″	59°55′36″	54°54′11″	48°35′25″	43°48′47″
$S_1(t_1)$ (m)	0.792945	0.787394	0.782800	0.778960	0.773080	0.766664	0.765147	0.768314	0.779317	0.789723
$\Delta S_1(t_1)$ (m)	0.007055	0.012606	0.017200	0.021040	0.026920	0.033336	0.034853	0.031686	0.020683	0.010277
$dist_{\Delta S_1>0.01}$ (m)	+	7	15.25	20	25.25	29.75	31.25	30.75	25.5	3.25
$dist_{\Delta S_1>0.02}$ (m)	+	+	+	1.5	8.75	14.75	16.5	15.25	1.75	+
$dist_{\Delta S_1>0.03}$ (m)	+	+	+	+	+	3.25	5.0	2.0	+	+
PTI	6,048	5,994	6,076	6,081	6,169	6,290	6,393	6,540	6,799	6,924
PTII	6,207	6,403	6,555	6,674	6,870	7,170	7,286	7,611	8,098	8,398
PTIII	6,516	6,816	7,062	7,254	7,417	7,927	8,328	8,683	9,382	9,861

Table 2: Test results for the stands behind the goal (for $\Delta x \in \{0.5, 1, 1.5, 2, 3, 5, 7, 10, 15, 20\}$, $n, m, k = 25$)

Δx (m)	**0.5**	**1**	**1.5**	**2**	**3**	**5**	**7**	**10**	**15**	**20**
a_{A_1} (m)	66.3	66.8	67.3	67.8	68.8	70.8	72.8	75.8	80.8	85.8
b_{A_1} (m)	365.69134	260.29010	213.87164	186.36042	153.99161	122.04356	105.42506	91.00067	77.99210	70.63463
v_1 [°]	7°5′2″	9°59′11″	12°11′33″	14°2′5″	17°4′57″	21°47′12″	25°28′28″	29°55′35″	35°39′33″	40°7′9″
$S_1(v_1)$ (m)	0.795898	0.793302	0.791561	0.790433	0.789478	0.790640	0.793516	0.797715	0.799885	0.796214
$\Delta S_1(v_1)$ (m)	0.004102	0.006698	0.008439	0.009567	0.010522	0.009360	0.006484	0.002285	0.000115	0.003786
$dist_{\Delta S_1>0.01}$ (m)	+	+	+	+	1.25	+	+	+	+	+
PTI	4,185	4,248	4,288	4,327	4,397	4,482	4,471	4,647	4,930	5,248
PTII	4,428	4,593	4,627	4,660	4,845	5,126	5,361	5,677	6,037	6,499
PTIII	4,680	4,810	5,002	5,163	5,437	5,853	6,103	6,581	7,128	7,758

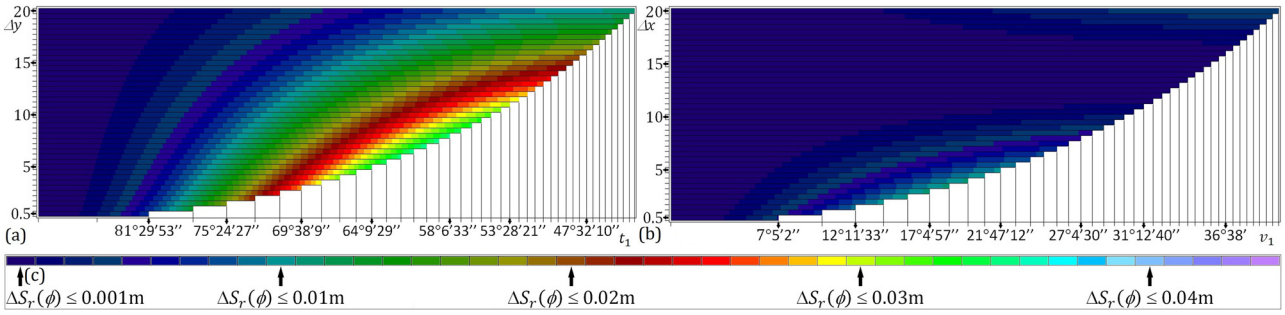

Figure 8: The depth of the first row in the stands: (a) BAI, BBI (for $\Delta y \in \{0.5, 1, 1.5, 2, \ldots, 20\}$), (b) AAI, ABI (for $\Delta x \in \{0.5, 1, 1.5, 2, \ldots, 20\}$), and (c) color palette.

stand BBI in the first row (for $\phi = 59^\circ 55' 36''$). The values of $\Delta S_r(\phi)$ can be reduced by moving the center of the ellipses e_{B_i} (e_{A_i}). Figure 7(d and e) illustrates the arrangement of seats in the stands.

Table 1 presents test results for the side stands (for the values $\Delta y \in \{0.5, 1, 1.5, 2, 3, 5, 7, 10, 15, 20\}$, n, m, $k = 25$). Since the greatest deficit $\Delta S_r(\phi)$ for the considered stadium stands always occurred for $\phi = t_1$ in the first row, the values of b_{B_1} (a_{B_1}), $S_1(t_1)$, $\Delta S_1(t_1)$, $dist_{\Delta S_1 > 0.01}$ (it is the number of meters in the first row, where $\Delta S_1(\phi) > 0.01$ m), $dist_{\Delta S_1 > 0.02}$, $dist_{\Delta S_1 > 0.03}$) were given for the first row. The values of PTI (it is the number of seats in the stands $2 \cdot$(BAI+BBI)), PTII, and PTIII are indicative and were determined as follows. (a) First, the stands BA and BB were divided into sectors (Figure 7(b and d)). That is, for each ring (I, II, and III), the angles μ_i (defining the centers of the stairs) were determined as follows. In the last row of each ring (starting at $\phi = 90^\circ$, along a broken line inscribed in the ellipse arc generating the back edge of the row), 14 times the 0.5 m long segment (0.5 m for 14 people in a row (compared with ref. [11], p. 14)) was measured. Next, the operations listed below were repeated until the angle t_1 was reached: once the 1.2 m long segment (for stairs (compared with ref. [9], p. 203)) and 28 times the 0.5 m long segment (0.5 m for 28 people in a row (compared with ref. [11], p. 14)) were measured and (in the middle of the stairs) the consecutive angle μ_i was determined and remembered. In lower rows, the established angles μ_i were used and care was taken to ensure that the stairs were 1.2 m wide (at the expense of seats in sectors) (Figure 7(d and e)). (b) Next, in each row of each sector, the number of segments with a length of 0.5 m was counted (one seat = 0.5 m). Entrances, the television, press and VIP areas were omitted. The number of seats PT (for the entire stadium for $n, m, k = 25$) was determined for $\Delta y = 0.5$ and $\Delta x = 10$.

$$\begin{aligned} \mathrm{PT} &= 2 \cdot [2(\mathrm{BA} + \mathrm{BB})] + 2 \cdot [2(\mathrm{AA} + \mathrm{AB})] + 4 \cdot [C] = \\ &= 2 \cdot 18{,}771 + 2 \cdot 16{,}905 + 4 \cdot 3{,}395 = 84{,}932 \end{aligned}$$

Table 2 presents test results for the stands behind the goal. Figure 8 illustrates the values of $\Delta S_1(\phi)$ for the first rows of stands (a) BAI, BBI, (b) AAI, ABI (for Δx, $\Delta y \in \{0.5, 1, 1.5, 2, \ldots, 20\}$). The values of Δx and Δy increase every 0.5 m. The row depth $S_1(\phi)$ was measured for the points P_i determined every $\Delta\phi_i = \text{const} = 0.05^\circ$ (P_i lie on the arc of the ellipse e_{B_i} (e_{A_i}) defining the back edge of the first row). The reader can compare the floor colors in the first row in Figure 7(a and b), the belt colors for $\Delta y = 7$ m (in Figure 8(a)), and the belt colors for $\Delta x = 3$ m in Figure 8(b).

3.3 Lines of sight of the focus point

The *focus* is a point on the pitch of which unobstructed vision provides a full view of the entire playing field. In the case of a football arena, this is usually the closest point on the sideline. The observation of this point is possible only when the line of sight connecting this point with the point of the observer's eye (let us denote by P_{Fi}) runs tangent to the top of the viewer's head (from the row below) or above it (compared with ref. [9], p. 97, Figure 9(b)). We propose a simple algorithm (determining the optimal height of the ring steps), which ensures an unobstructed view of each point of the pitch from any point of the stands shaped by ellipse arcs.

The *line of sight correction* (LSC) *algorithm* determines the optimal height H_n of the steps of the ring, i.e., such a minimum value (identical for the entire ring) that it is possible to observe the entire playing field from any eye point of the ring. The LSC algorithm is based on the *method of the farthest eye point* (a graphical method of modeling a rectilinear profile of the spectator stand (compared with ref. [9], p. 134)) and is adapted to the stands shaped by ellipse arcs. The LSC algorithm optimizes the *initial lines of sight of the focus point F* (ILSF is the line of sight lying on the plane (containing

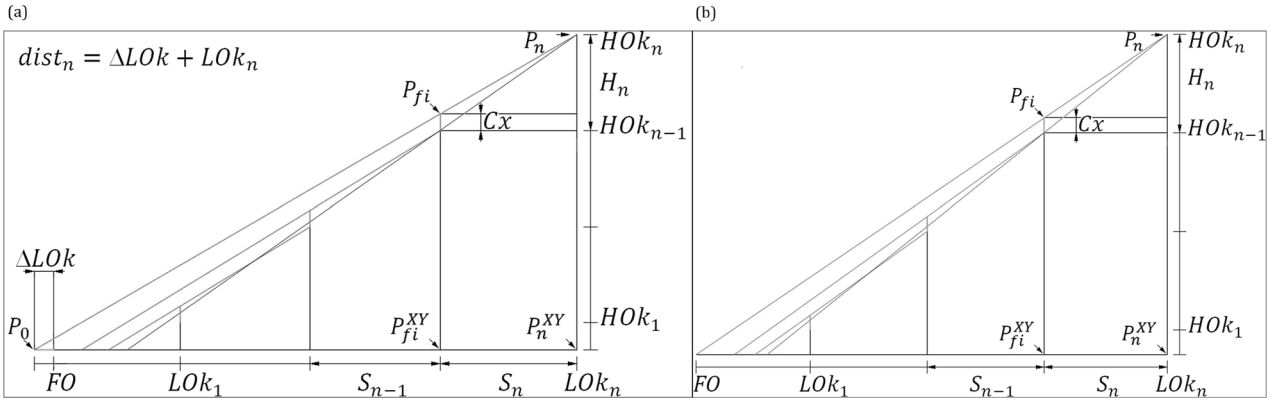

Figure 9: The profile of the stand BBI (for $n = 4$) in the plane (containing two points P_n, *FO*, and perpendicular to the *OXY* plane): (a) for the approximate value of H_n and (b) for H_n determined by the LSC algorithm.

two points P_{Fi} and F and perpendicular to the *OXY* plane) passing through two points: the observer's eye point P_{Fi} and the top of the viewer's head P_{fi} from the previous row). In Figure 9(a and b), the ILSF lines are colored in red, P_n – the observer's eye point from the row n. Two types of focus points were analyzed: (a) *FO* (the closest point on the nearest sideline), and (b) *FL*, *FR* (the two closer corners of the playing field).

The LSC algorithm (the variant for the stand BBI)

Focus – the point *FO*(*dx*, *dy*, 0) at the corner of the playing field (Figure 10).

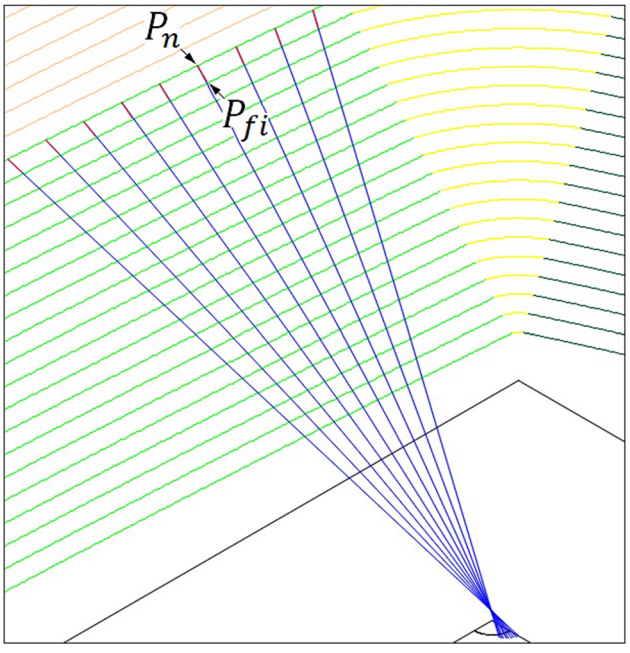

Figure 10: ILSF lines for the *n*th row in the stand BBI, Focus – the point *FO*(*dx*, *dy*, 0).

Initialization:

```
( 1) double Cx = 0.12, HnB = Cx+0.00001;
( 2) double HOkn = HOk1+(n-1)*HnB, h = HOkn;
( 3) double b = day+dlt_y, t1 = asin(day/b);
( 4) double a = dax/cos(t1)+dlt_Ok, b += dlt_Ok;
( 5) double an = a+(n-1)*S, bn = b+(n-1)*S;
( 6) double ai = an-S, bi = bn-S, u = acos(dx/an);
( 7) ellipse* ellB = new ellipse(an,bn);
```

Iterations:

```
( 8) while (u >= t1){
( 9)   xn = an*cos(u); yn = bn*sin(u); zn = h;
(10)   A1 = xn-dx; B1 = yn-dy;
(11)   A = pow(bi*A1,2)+pow(ai*B1,2);
(12)   B = pow(bi,2)*2*dx*A1+pow(ai,2)*2*dy*B1;
(13)   C = pow(bi*dx,2)+pow(ai*dy,2)-pow(ai*bi,2);
(14)   D = B*B-4*A*C;
(15)   if(D >= 0){
(16)     h1 = (-B+sqrt(D))/(2*A);
(17)     fi = acos((dx+h1*(xn-dx))/ai);
(18)     xfi = ai*cos(fi); yfi = bi*sin(fi);
                           zfi = h-HnB+Cx;
(19)     Sn = sqrt(pow(xn-xfi,2)+pow(yn-yfi,2));
(20)     LOkn = sqrt(pow(xn-dx,2)+pow(yn-dy,2));
(21)     distn = ((HOk1+(n-1)*HnB)*Sn)/(HnB-Cx);
(22)     if (LOkn-distn < 0){
(23)       distn = LOkn;
(24)     HnB =
           (distn*Cx+HOk1*Sn)/(distn-Sn*(n-1));}}
(25)   xy = ellB->Node_ellipse_prev((u*180)/
           PI,0.25);
(26)   u = acos(xy->x/an); delete xy;}delete ellB;
(27) Hn = HnB;
```

Description of the LSC algorithm: In the LSC algorithm, all distances are measured on a plane containing two points P_n and FO and perpendicular to the OXY plane. The points $P_n(x_n, y_n, z_n)$, $P_{fi}(x_{fi}, y_{fi}, z_{fi})$ (respectively in the nth and $(n-1)$th row) lie on one initial line of sight of the focus point FO (in Figure 10, the segments $\overline{P_nP_{fi}}$ are red). The point P_n lies on the eye line in the nth row (the ellipse arc $e_{\Delta B_n}$) at the height HOk_n, and the point P_{fi} lies above the eye line in the $(n-1)$th row (the ellipse arc $e_{\Delta B_{n-1}}$) at the height $HOk_{n-1} + Cx$. P_n^{XY} is the orthographic projection of the point P_n onto the OXY plane.

Symbols in the algorithm (Figure 9): `LOkn` ($LOk_n = |\overline{P_n^{XY}FO}|$) – the horizontal distance of the eye point P_n from the focus point FO; `distn` ($dist_n = |\overline{P_n^{XY}P_0}|$) – the horizontal distance of the eye point P_n from the point $P_0(x_0, y_0, z_0)$ (an intersection of the ILSF line with the plane of the pitch); `Sn` ($S_n = |\overline{P_n^{XY}P_{fi}^{XY}}|$) – the horizontal distance of the eye point P_n from the point P_{fi}; `HnB` – the height of the ring steps (the auxiliary variable); `Hn` (H_n) – the optimal height of the ring steps (the return value); `HOk1` (HOk_1) – the elevation of the eye point of the first row; `HOkn` (HOk_n) – the elevation of the eye point of the nth row; `an` ($a_{\Delta B_n}$) – the semi-major axis of the ellipse $e_{\Delta B_n}$; `ai` ($a_{\Delta B_{n-1}}$) – the semi-major axis of the ellipse $e_{\Delta B_{n-1}}$.

Initialization: As the initial value of `HnB`, any value from the range $(Cx, H_n]$ can be taken.

Iterations: The LSC algorithm makes calculations for the consecutive eye points P_n (on the ellipse arc $e_{\Delta B_n}$ for $u \in [\arccos\left(\frac{dx}{a_{\Delta B_n}}\right), t_1]$ – the variant BBI) measured every 0.25 m, along a broken line inscribed in the ellipse arc (in Figure 10, points P_n were measured every 2 m). For each eye point P_n, the LSC determines the eye point P_{fi} (in the $(n-1)$th row (lines 10–18)) and distances S_n, LOk_n, $dist_n$ as follows.

The ellipse $e_{\Delta B_n}$: $x_n = a_{\Delta B_n}\cos(u)$, $y_n = b_{\Delta B_n}\sin(u)$.

Let us write down the equations of the line l^{XY}, which is the orthographic projection of the line l (passing through the points $P_n(x_n, y_n, z_n)$ and $FO(dx, dy, 0)$) onto the OXY plane and determine the coordinates x_{f_i}, y_{f_i} of the point $P_{f_i}^{XY}$ (an intersection of the line l^{XY} with the ellipse $e_{\Delta B_{n-1}}$).

$$x_{f_i} = dx + h_1(x_n - dx) = a_{\Delta B_{n-1}}\cos(\varphi),$$
$$y_{f_i} = dy + h_1(y_n - dy) = b_{\Delta B_{n-1}}\sin(\varphi).$$

We determine h_1 (as in the program (lines 10–16)) and obtain the coordinates of the point $P_{f_i}^{XY}$. Next, we calculate the lengths of $S_n = |\overline{P_n^{XY}P_{f_i}^{XY}}|$ (line 19) and $LOk_n = |\overline{P_n^{XY}FO}|$ (line 20). The value of $dist_n$ (line 21) results from the following equation:

$$\frac{HOk_n}{HOk_n - H_n + Cx} = \frac{dist_n}{dist_n - S_n}, \tag{10}$$

where $HOk_n = HOk_1 + (n-1)H_n$ (Figure 9(a)) for H_n = `HnB` (current value). If $(LOk_n - dist_n < 0)$ (i.e., the ILSF line is over the focus point FO (line 22)), the `HnB` value should be increased. The LSC algorithm optimizes the value of $dist_n$ to LOk_n (=$|\overline{P_n^{XY}FO}|$ – the optimal value) and for the new $dist_n$ determines `HnB` from the equation (10) (Figure 9(b)). Then

$$\mathsf{HnB} = H_n = \frac{dist_n \cdot Cx + HOk_1 \cdot S_n}{dist_n - (n-1)S_n}.$$

Remark 3. (a) The *critical point* P_{n_k} is the eye point (in the nth row of the stand BBI), for which the optimal value of H_n was determined.
(b) The optimal value of H_n (for the critical point P_{n_k}) guarantees that the focus FO will be visible to all eye points from the stand BBI, provided that the following condition is met:

$$\frac{S_{n-1}}{S_n} \le \frac{(HOk_{n-1} + Cx)}{HOk_{n-1}}, \tag{11}$$

where S_n and S_{n-1} (the depths of the nth and $(n-1)$th rows, respectively) are determined for the critical point P_{n_k}.

It was checked that for the stands BBI (and ABI) (for $\Delta x,\ \Delta y \in \{0.5, 1, 1.5, 2, \ldots, 20\}$, $n = 20$, $HOk_1 = 2$ m, $Cx = 0.12$ m), the condition $\frac{S_{i-1}}{S_i} \le \frac{(HOk_{i-1}+Cx)}{HOk_{i-1}}$ is fulfilled for all rows $i = 3, \ldots, n$. For the aforementioned stands, the height H_n determined for the critical point P_{n_k} (from the nth row) is sufficient to make the point FO visible from any eye point in these stands.

In order to determine the optimal value of H_n, we have to execute the LSC algorithm (after appropriate modifications in determining the coordinates of the point $P_{f_i}^{XY}$) from each point P_n (from the nth row) of the stands BAI, BBI, AAI, ABI, and CI, and select the largest value of H_n.

In Figure 11(a), the ILSF lines for the focus FO (in the stands BAI, BBI, AAI, ABI, and CI, for all rows) are plotted. We can see that the height H_n (determined by the LSC algorithm) guarantees seeing the closest point on the nearest sideline from each eye point in the aforementioned stands. Figure 11(b) presents the ILSF lines for the focus point FO (in the stands BA, BB, AA, AB, and C, for all rows $(n, m, k = 20)$). For each ring, the optimal height of steps (H_n, H_m, and H_k) was determined. In each row, the ILSF lines are painted in a different color (according to the color palette).

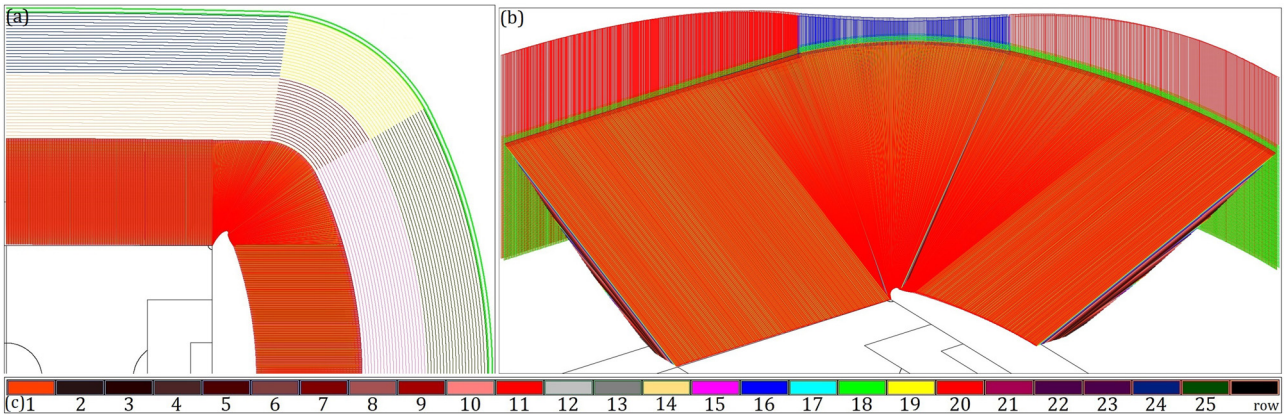

Figure 11: Lines ILSF for the focus point *FO*: (a) in the stands BAI, BBI, AAI, ABI, and CI (for n rows), (b) in the stands BA, BB, AA, AB, and C (for $R = n + m + k$ rows), and (c) color palette.

Tests showed that in the case of the proposed stands (shaped by arcs of ellipses), seeing the focus *FO* (the closest point on the nearest sideline) from any eye point in the stands does not guarantee seeing the focuses *FL* and *FR* (the closer corners of the playing field). Figure 12 is plotted for all rows in all stands (for $HOk_1 = 2$ m, Δx, $\Delta y = 0.5$). In Figure 12(a), the value of H_n (H_m, H_k) was calculated using the LSC algorithm for the focus *FO*; hence, the ILSF lines intersect the sideline (H_n is not sufficient). In Figure 12(b), the value of H_n (H_m, H_k) was calculated using the LSC algorithm for the focuses *FL* and *FR* (the ILSF lines do not cross the sideline). The ILSF lines where the eye point P_{Fi} is in the stand C and the point P_{fi} is in the stand BB (or AB) are plotted in black.

To find the optimal value of H_n, we have to execute the LSC algorithm (for the focuses *FL* and *FR*) from each point P_n (from the nth row) of the stands BAI, BBI, AAI, ABI, and CI, and select the largest value of H_n. In addition, we need to check (a) the ILSF line (passing through the eye point P_n (in the stand CI) and the point P_{fi} (in the stand BBI)) for the focus *FL* and (b) the ILSF line (passing through the eye point P_n (in the stand CI) and the point P_{fi} (in the stand ABI)) for the focus *FR*.

Table 3 presents the optimal heights of the ring steps for the stadiums with the following parameters ($\Delta x = 10$, $\Delta y \in \{0.5, 1, 2, \ldots, 10\}$, $HOk_1 = 1.2$ m, $n, m, k = 20$). The values of $H_n(FO)$ were determined for the focus *FO*, the values of $H_n(FRFL)$ were obtained for the focuses *FL* and *FR* and HOk_n is the elevation of the eye point of the nth row (determined for the optimal H_n). Analogous calculations were made for rings II and III.

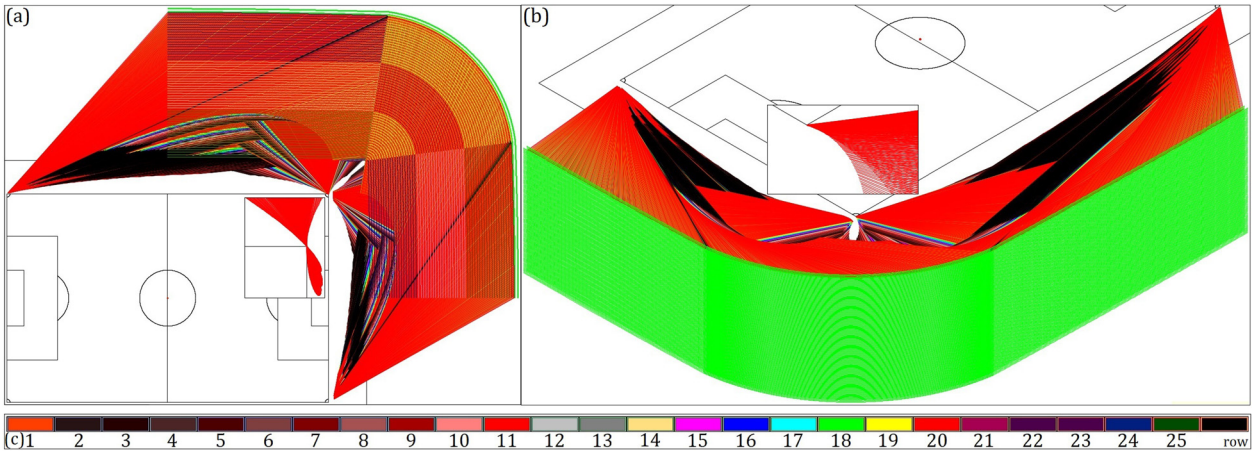

Figure 12: ILSF lines (plotted for the focuses *FL*, *FR*) for all eye points in all stands for the values of H_n, H_m, H_k determined by the LSC algorithm for focuses (a) *FO*, (b) *FL*, *FR*, (c) color palette.

Table 3: Heights for rings I, II, and III (for $\Delta x = 10$, $\Delta y \in \{0.5, 1, 2, \ldots, 10\}$, $HOk_1 = 1.2$, $n, m, k = 20$)

Δy	0.5	1	2	3	4	5	6	7	8	9	10
$H_n(FO)$	0.356464	0.352438	0.345274	0.338902	0.333097	0.327733	0.32273	0.318034	0.313665	0.309664	0.306011
$H_n(FLFR)$	0.357095	0.353325	0.34622	0.339649	0.333574	0.327964	0.322792	0.318034	0.313665	0.309664	0.306011
HOk_n	7.98481	7.91317	7.77818	7.65334	7.5379	7.43131	7.33305	7.24264	7.15963	7.08362	7.01421
$H_m(FO)$	0.428275	0.424208	0.416733	0.409817	0.403307	0.397131	0.391257	0.385756	0.38065	0.375925	0.37157
$H_m(FLFR)$	0.428828	0.424915	0.417365	0.410215	0.40348	0.397162	0.391257	0.385756	0.38065	0.375925	0.37157
HOk_m	16.5614	16.4115	16.1255	15.8576	15.6075	15.3745	15.1582	14.9578	14.7726	14.6021	14.4456
$H_k(FO)$	0.473431	0.469526	0.46215	0.455112	0.448332	0.4418	0.435615	0.429812	0.424388	0.41934	0.414659
$H_k(FLFR)$	0.473916	0.470084	0.462548	0.455287	0.448362	0.4418	0.435615	0.429812	0.424388	0.41934	0.414659
HOk_k	26.0397	25.8132	25.3765	24.9634	24.5747	24.2105	23.8705	23.554	23.2604	22.9889	22.7388

3.4 The borderline position of the eye

European Standard EN 13200-1 specifies the maximum range of sight (RS = 190 m) for football stadiums. For this distance, the minimum angle of view of the ball (with a diameter of 0.22 m) is $\psi = 0^\circ 4'$ (compared with ref. [13], p. 84, 85). The height of the eye point in the last row can reach up to 45 m (above the arena level). Hence, the line of sight of the farthest point of the playing field can be sloped at a large angle. Therefore, the actual length of the segment (from the point of the farthest eye (raised to the height of HOk_k) to the farthest corner of the playing field) is important (compared with ref. [9], p. 89).

The *ball vision verification algorithm* (in short BVV). The variant for the stand C.

(a) Plot a fragment of the sphere e_ψ (compared with (12)) with a radius of RS = 190 m and the center at the farthest corner of the playing field.

$$e_\psi: \; x_\psi = a_\psi \cos(u)\sin(v) - dx, \quad y_\psi = a_\psi \sin(u)\sin(v) - dy, \quad z_\psi = a_\psi \cos(v), \tag{12}$$

$$P_{Fi1}: \; x_{Fi1} = a_{\Delta C_i}\cos(\varphi_1) + dax, \quad y_{Fi1} = a_{\Delta C_i}\sin(\varphi_1) + day, \quad z_{Fi1} = HOk_i, \tag{13}$$

$$P_{Fi2}: \; x_{Fi2} = a_{\Delta C_i}\cos(\varphi_2) + dax, \quad y_{Fi2} = a_{\Delta C_i}\sin(\varphi_2) + day, \quad z_{Fi2} = HOk_i. \tag{14}$$

(b) Determine on the eye line in the ith row (the ellipse arc $e_{\Delta C_i}$ (compared with Section 3.1)) two eye points P_{Fi1} and P_{Fi2} (compared with (13) and (14)) adjacent to each other (at a distance of 0.25 m). HOk_i – the elevation of the eye point in the ith row. (c) Determine the point $P_{Fi1\psi}(x_{Fi1}, y_{Fi1}, z_{P_{Fi1\psi}})$ – an intersection of the line h_{φ_1} (passing through the points P_{Fi1} and P^{XY}_{Fi1}) with the sphere e_ψ. The point P^{XY}_{Fi1} is the orthographic projection of the point P_{Fi1} onto the OXY plane. In the same way, determine the point $P_{Fi2\psi}(x_{Fi2}, y_{Fi2}, z_{P_{Fi2\psi}})$ (an intersection of the line h_{φ_2} with the sphere e_ψ). (d) If the condition

$$\left(z_{P_{Fi1\psi}} \geq HOk_i \text{ and } z_{P_{Fi2\psi}} \geq HOk_i\right) \tag{15}$$

is met, then the segment $\overline{P_{Fi1}P_{Fi2}}$ (in the ith row) is inside the sphere e_ψ (it is within the range of view of RS). Then the color of the segment follows the color of the eye line in the stand. Otherwise, the segment $\overline{P_{Fi1}P_{Fi2}}$ is outside the range of view RS (the segment is red).

The aforementioned algorithm should be repeated for consecutive pairs of points P_{Fi1} and P_{Fi2} adjacent to each other in the ith row (for $i = n + m + k, \ldots, q$, where q is the first row (from the top) in which for all pairs of points P_{Fi1} and P_{Fi2} the condition (15) is met). Figure 13(a) shows

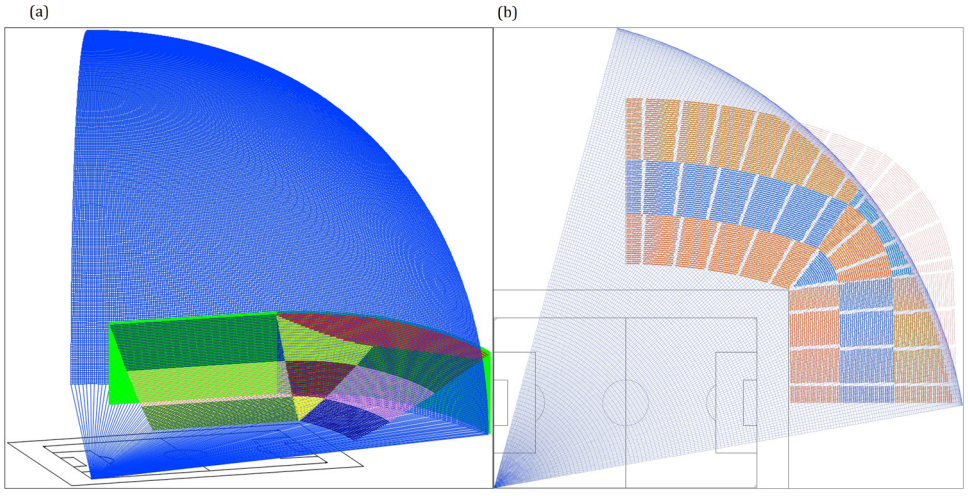

Figure 13: (a) Borderline positions of the eye lines (for RS = 175 m) and (b) stadium stands with 81,928 seats.

the eye lines in the stands (Δx = 10, Δy = 0.5, HOk_1 = 1.2, n, m, k = 20). The places where the range of sight RS = 175 m was exceeded are marked in red.

The largest football stadiums (except Salt Lake Stadium (Kolkata)) have a capacity of up to 100,000 seats. It has been checked that verified stadium (stadium template) can accommodate up to 82,000 seats (orange and blue seats in Figure 13(b)). It was assumed that each spectator (each point of the eye) must see the entire playing field from a distance of up to 190 m. The stadium stands (in Figure 13(b)) were plotted for the following parameters: Δy = 10 m, Δx = 0.5 m, n = 25, m = 27, k = 31, H_n = 0.365873 m, H_m = 0.445959 m, H_k = 0.501235 m, HOk_1 = 1.2 m, HOk_n = 9.98094 m, HOk_m = 22.0218 m, HOk_k = 37.5601 m, and the number of seats: 81,928.

3.5 Plotting a profile of the stadium

Figure 14 shows a vertical plane containing the points $T_R(\phi)$ and T_{R-1} ($T_R(\phi)$ – the point on the ellipse arc e_{B_R} for the angle ϕ = 85° (at the height equal to HOk_k – 1.2 m); T_{R-1} – the point on the ellipse arc $e_{B_{R-1}}$ (at the height equal to $HOk_k - H_k$ – 1.2 m), the segment $\overline{T_R^{XY} T_{R-1}^{XY}}$ is perpendicular to the ellipse e_{B_R} (i.e., perpendicular to the back edge of the last row), $R = n + m + k$). The row depths S_i and the horizontal distances between P_{Fi} (the eye point in ith row) and P_{Fi-1} (the eye point in $(i-1)$th row) were determined using the formulas (compared with (9), Section 2.4). The heights of the steps of the rings are constant (different for each ring): H_n = 0.357095 m, H_m = 0.428828 m, H_k = 0.473916 m, and

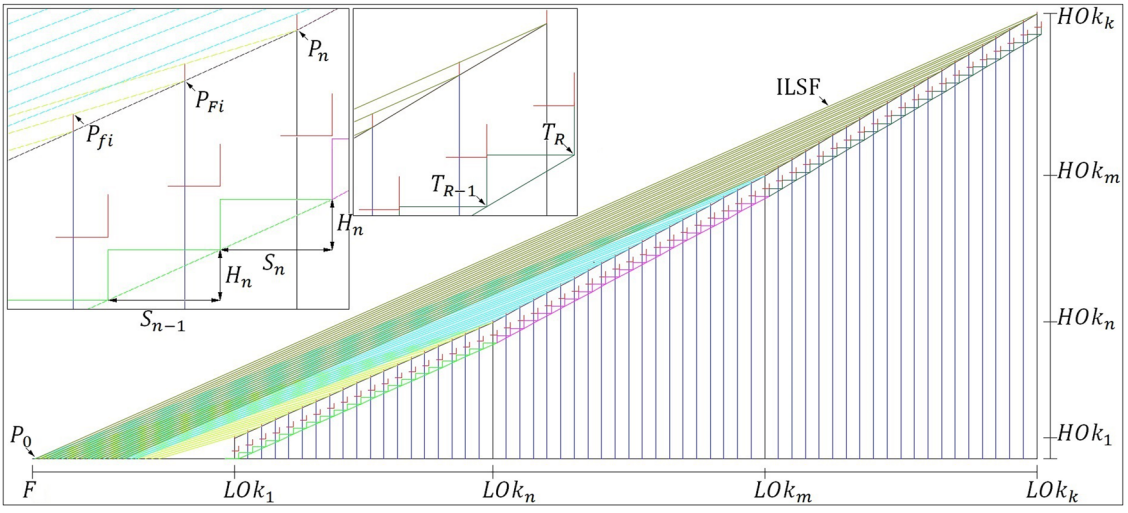

Figure 14: The profile of the stand BA (Δx = 10 m, Δy = 0.5 m, n, m, k = 20, HOk_1 = 1.2 m, Cx = 0.12 m, and ϕ = 85°).

HOk_k = 26.039685 m. Figure 14 shows the ILSF lines for the focus F (the point on the nearest sideline).

3.6 Row depth correction

In Section 3.2, the depth $S_r(\phi)$ and the deficit $\Delta S_r(\phi)$ were measured (for the row r and the angle ϕ) along a line perpendicular to the back edge of the row. Figure 7 shows the stadium stands for unfavorable values Δx = 3 m and Δy = 7 m (where $\Delta S_1(\phi)$ = 0.034853 m for $\phi = 59^\circ 55' 36''$). To correct the depth $S_r(\phi)$, we have to move the center of ellipses. Figure 15 shows the top view of the stands BA and BB. Virtual arcs of ellipses e_{B_i} ($i = 0, \ldots, 60$) (representing the front and back edges of 60 rows of the stands BA, BB) were connected by colored segments (perpendicular to the back edges) measured every 0.05 m. The segments were colored depending on the length $S_r(\phi)$ (according to the color palette (Figure 15(c))).

The *row depth correction* (RDC) *algorithm* corrects the values of $S_r(\phi)$ in all rows of stands BA, BB with the desired accuracy ΔE. Let us note (Figure 15) that it is enough to correct the value of $S_1(t_1)$, i.e., the length of the segment $\overline{P_{Fi}P_{fi}}$ (where P_{Fi} is a point on the ellipse arc e_{B_1} (for the angle $\phi = t_1$), P_{fi} is a point on the ellipse arc e_{B_0}, and the segment $\overline{P_{Fi}P_{fi}}$ is perpendicular to the arc e_{B_1}).

The RDC algorithm

```
( 1) double dlt_E = 0.00001, dlt_b = 0;
( 2) while (true){
( 3)   b = day+dlt_y+dlt_b; t1 = asin((day+dlt_b)/b);
( 4)   a = dax/cos(t1);
( 5)   ai = a+S; bi = b+S; ell1 = new ellipse(ai,bi);
( 6)   xFi = ai*cos(t1); yFi = bi*sin(t1)-dlt_b;
( 7)   Pfi =
         ell1->Node_ellipse_xQ2yQ2((t1*180)/PI,S);
( 8)   S1 = sqrt(pow(xFi-Pfi->x,2)+
                  pow((yFi-(Pfi->y-dlt_b)),2));
( 9)   delete Pfi; delete ell1;
(10)   if((S-S1) <= dlt_E) break; dlt_b += 1;}
```

The RDC algorithm determines the value of Δb_B (an increment of the semi-minor axis of the ellipse e_{B_i}) by which the center of the ellipses e_{B_i} should be shifted. At initialization, we set the values ΔE = 0.00001 m and $\Delta b_B = 0$. In consecutive iterations, the algorithm determines: the length of the semi-minor axis b_{B_0} (for the current value of the increment Δb_B), the coordinates of points P_{Fi} and P_{fi} (lines 6 and 7), the value of $S_1(t_1)$ (line 8) and checks the condition ($S - S_1(t_1) \le \Delta E$). If the condition is met, the algorithm exits the loop. Otherwise, it increases the value of Δb_B by 1 m and repeats the calculations for the semi-minor axis b_{B_0} longer by 1 m. The coordinates of the point P_{fi} are determined from the formula (9) (compared with Section 2.4).

For stands BA and BB (for n, m, k = 20, Δx = 3 m, Δy = 7 m), with a given accuracy of ΔE = 0.00001 m, the RDC algorithm determined the value of Δb_B = 240 m. For $\Delta b_B = 0$ (before the correction), the angle $t_1 = 59^\circ 55' 36''$ and the maximum value of $\Delta S_1(t_1)$ = 0.034853 m (Figure 15(a)). After the correction (for Δb_B = 240 m) the angle $t_1 = 77^\circ 25' 45''$ and the maximum value of $\Delta S_1(t_1)$ = 0.000009 m (Figure 15(b)). Figure 15(b) shows how the lengths of $S_1(\phi)$ (in the first row) were changed for $\phi \in [t_1, 90^\circ]$. The first belt (from the bottom) corresponds to the value $\Delta b_B = 0$ and each

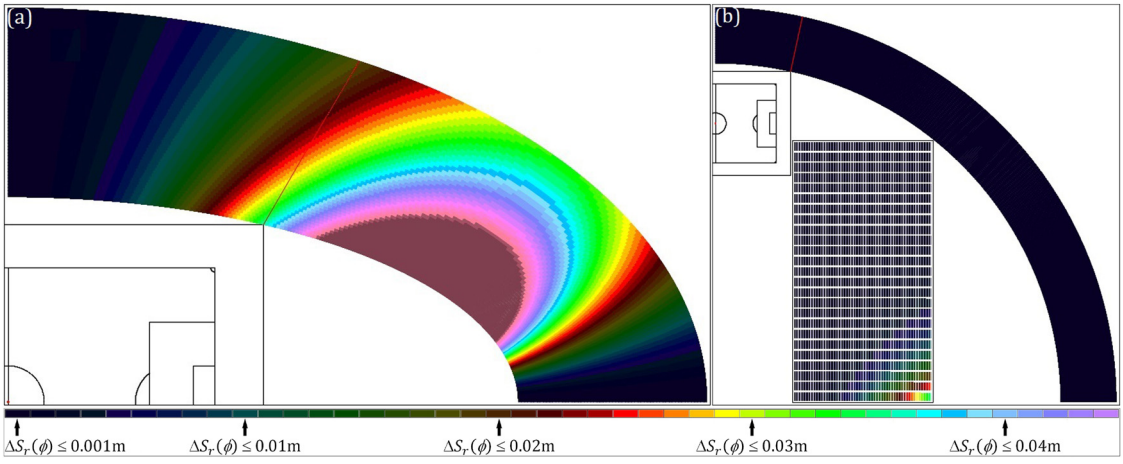

Figure 15: The stands BA, BB: (a) top view, (b) top view (corrected), and (c) color palette.

next one was determined for the semi-minor axis b_{B_0} increased by 10 m.

4 Applications of the method

Nowadays, designers are looking for more and more sophisticated forms for representative architectural objects (Sydney Opera House, Cayan Tower (Dubai), 30 St Mary Axe (London), La Seine Musicale (Paris)). The designing of such objects requires appropriate design technologies, including ones for creating virtual prototypes, simulations, and numerical and visual data analysis. Also, when designing less impressive buildings, it is important to be able to obtain mathematical models for individual elements, fully dimension them, change the parameter values at each stage, and immediately obtain their visualization and a numerical report.

The presented geometric method can be used to model fragments of architectural objects with an ellipsoidal shape (elevations, roofs, and domes). Light lattice structures (compared with ref. [14]) or reinforced double-layer lattice structures (compared with ref. [7,15]) are especially appreciated. The method provides mathematical formulas for the coordinates of points and angles for the base surface and various surfaces approximating it. The proposed technique (programing DXF files) provides visualization (in the AutoCAD system) and full dimensioning (in TXT file). The combination of these methods can help designers effectively. We can find a lot of the Computer-aided design systems (CATIA, Digital Project, Pro/ENGINEER) that include parametric design tools and offer designers the possibility to create parametric scripts. But it is very expensive software. Only large design companies can afford to buy it. The proposed technology is much cheaper and allows the programer to design complex curvilinear forms in a short time (e.g., an ellipsoidal stadium with stands shaped by ellipse arcs).

5 Summary

The problem of placing up to 82,000 of people in the stands (with rows along the arcs of ellipses) of the stadium has been resolved. The problem is very precisely defined due to the established norms (compared with ref. [10,11]). First, the analysis of the depth of the rows was carried out. Next, a comfortable space was provided for each seat (in all stands) with an accuracy of 0.000009 m (compared with the RDC algorithm). An unobstructed view of the entire playing field from any place in the stands (at a distance not exceeding 190 m) was ensured, using the LSC algorithm and the BVV algorithm. The mentioned algorithms are effective because the formula (9) was used. In addition, the elevation of the stadium (in the shape of an ellipsoid) made of a light, two-layer lattice (Figure 1) was proposed. The design is a template (can be used for different parameter values). The geometric method and programing of DXF files with visualization in the AutoCAD system were used.

Conflict of interest: The author states no conflict of interest.

Data availability statement: All data generated or analyzed during this study are included in this published article (and its supplementary information files).

References

[1] AutoCAD (2012) DXF Reference. Published by AutoDesk Inc. San Rafael. USA. 2011.
[2] Kowalski M. Cyclometric functions formulas (with proofs). 2012. Available from: https://www.kowalskimateusz.pl/materialy/wzory3.1.pdf.
[3] Borowska A. Approximation of the ellipse offset curves in turbo roundabouts design. The Journal Biuletyn of Polish Society for Geometry and Engineering Graphics. 2018;31:43–51.
[4] Koźniewski M. Thickness analysis of a saddle. The Journal Biuletyn of Polish Society for Geometry and Engineering Graphics. 2016;28:25–32.
[5] Pottmann H, Asperl A, Hofer M, Kilian A. Architectural geometry. Pennsylvania, USA: Bentley Institute Press. 2007.
[6] Grabowski R. Ellipse offset curves in the formation of turbo-roundabouts. Roads and Bridges – Drogi i Mosty. 2015;14:193–202.
[7] Koźniewski E, Borowska A. Hyperboloid offset surface in the architecture and construction industry. Open Engineering. 2019;9:404–14.
[8] Grzegorczyk J. Mathematics. Publishing House of the Warsaw University of Technology. Warsaw; 1978.
[9] Pelczarski Z. Widownie współczesnych stadionów. Determinanty i problemy projektowe [Spectator Stands of Contemporary Stadiums. Determinants and Design Problems]. Oficyna Wydawnicza Politechniki Białostockiej. 2018.
[10] Polska Norma PN-EN 13200-1:2005. Obiekty widowiskowe. Cz. 1. Wymagania dotyczące projektowania widowni. Wyszczególnienie. Polski Komitet Normalizacyjny. grudzień; 2005.

[11] Wytyczne i Dobre Praktyki w Zakresie Infrastruktury Stadionowej oraz Organizacji Meczów Piłki Nożnej. Cz. 1. Infrastruktura Stadionowa. Departament Organizacji Imprez, Bezpieczeństwa i Infrastruktury. Polski Związek Piłki Nożnej. kwiecień 2016.
[12] Leja F. Rachunek różniczkowy i całkowy [Differential and integral calculus]. PWN. Warsaw. 1973.
[13] Pelczarski Z. The issue of the range of vision in design of grandstands at the contemporary stadiums. Advances in Social and Organizational Factors. Boca Raton: CRC Press; 2012;83–92.
[14] Gayakwad BR, Hiriyur A, Patil VV, Arjun K, Lakshmi S. Design considerations for a geodesic dome - a critical review. International Journal of Advances in Science Engineering and Technology. 2018;6(1):8–13.
[15] Bysiec D. The investigation of stability of double-layer octahedron-based geodesic domes. Structure and Environment. 2011;3(3):30–41.